

Article

Not peer-reviewed version

---

# Numerical Study of Sustainable Bio-Based Bricks with Integrated Phase Change Materials for Enhanced Thermal Performance

---

[Fabien Beaumont](#)\*, Guillaume Polidori, [Mohammed Lachi](#)

Posted Date: 4 June 2026

doi: 10.20944/preprints202606.0329.v1

Keywords: raw earth; phase change material; thermal performance; bio sourced materials



Preprints.org is a free multidisciplinary platform providing preprint service that is dedicated to making early versions of research outputs permanently available and citable. Preprints posted at Preprints.org appear in Web of Science, Crossref, Google Scholar, Scilit, Europe PMC, OpenAlex.

Copyright: This open access article is published under a [Creative Commons CC BY 4.0 license](#), which permit the free download, distribution, and reuse, provided that the author and preprint are cited in any reuse.

Disclaimer/Publisher's Note: The statements, opinions, and data contained in all publications are solely those of the individual author(s) and contributor(s) and not of MDPI and/or the editor(s). MDPI and/or the editor(s) disclaim responsibility for any injury to people or property resulting from any ideas, methods, instructions, or products referred to in the content.

Article

# Numerical Study of Sustainable Bio-Based Bricks with Integrated Phase Change Materials for Enhanced Thermal Performance

Fabien Beaumont \* Guillaume Polidori and Mohammed Lachi

Institut de Thermique, Mécanique et Matériaux (IThEMM), UFR Sciences Exactes et Naturelles, Université de Reims Champagne-Ardenne, 51100 Reims, France

\* Correspondence: fabien.beaumont@univ-reims.fr

## Abstract

Despite growing interest in sustainable construction materials, unfired clay bricks still exhibit limited thermal insulation performance. This study investigates the enhancement of perforated raw earth bricks through the integration of a bio-based phase-change material (PCM) derived from coconut oil to improve thermal damping and heat storage capacity. A numerical analysis was conducted on several configurations, including a solid reference brick, a hollow brick with air-filled cavities, and bricks incorporating one, two, or three rows of PCM encapsulated in polylactic acid (PLA) tubes. Results show a progressive improvement in thermal performance with increasing PCM content showing that the three-row PCM configuration achieved the best dynamic thermal behavior. Thermal gradient and enthalpy analyses revealed the combined effects of the thermal conductivity of PLA and raw earth and the latent heat storage capacity of the PCM. Replacing 17 PCM tubes with a single container of equivalent volume further improved performance while reducing system complexity and cost, decreasing the decrement factor by nearly 50% compared with the three-row configuration. These findings demonstrate the potential of PCM-enhanced raw earth bricks for passive thermal regulation in sustainable buildings, although experimental validation remains necessary.

**Keywords:** raw earth; phase change material; thermal performance; bio sourced materials

## 1. Introduction

The construction industry is currently experiencing a significant transformation driven by the urgent necessity to reduce greenhouse gas emissions and embrace circular economy principles. In this context, geosourced and biosourced materials are gaining recognition as credible alternatives to traditional construction materials like concrete and fired bricks, which are known for their high energy consumption and substantial CO<sub>2</sub> emissions during production. Among these sustainable options, unfired earth stands out due to its abundance, low embodied energy, local availability, and minimal processing requirements. Used for nearly 10,000 years [1,2], unfired earth remains one of the oldest and most widespread vernacular building materials. Today, approximately 8 to 10% of the global population—up to 25% in some developing countries—reside in earth-based dwellings [3]. Although its popularity waned during the twentieth century with the rise of industrialized concrete construction, recent renewed interest from scientific and technical perspectives has been spurred by decarbonization goals and the increasing integration of circular economy strategies within the construction sector [4–6].

Unfired earth can be applied through a variety of construction techniques tailored to local geography, climate, and cultural practices. Common load-bearing methods include adobe, rammed earth, and cob construction. Rammed earth involves compacting moist soil within formwork to create dense, monolithic walls with high thermal mass and adequate compressive strength [7]. Adobe bricks are produced by mixing clay-rich soil with water, then air-drying before use [8]. Another popular

technique involves compressed earth blocks (CEBs), made through mechanical compaction, which typically offers better uniformity and controlled mechanical properties. In their unstabilized form — without hydraulic binders or chemical additives—unfired earth bricks are highly environmentally friendly and fully recyclable. However, their sensitivity to water and relatively modest mechanical strength necessitate careful consideration during design and construction [9,10].

From a mechanical standpoint, adobe-like earth bricks typically exhibit compressive strengths ranging from 0.6 to 8.3 MPa [11–15], however, some recent experimental results have shown a narrower range of 1.03 to 4.80 MPa [6]. While these values are lower than those of conventional concrete, they can be sufficient for load-bearing applications when paired with appropriate structural solutions, such as increased wall thicknesses of around 30 centimeters and optimized masonry bonding techniques [16].

Beyond structural performance, the thermal properties of unfired earth are crucial in designing energy-efficient buildings. Thanks to their high density and specific heat capacity, earth materials provide significant thermal inertia, helping to dampen indoor temperature fluctuations. Incorporating plant fibers, like straw, can further reduce thermal conductivity and improve insulation, though this often comes at the expense of mechanical strength.

Generally, unfired earth demonstrates a high heat storage capacity and moderate thermal diffusivity, making it effective at moderating temperature swings within buildings [17]. However, its thermal conductivity—typically between 0.5 to 1.2  $\text{W}\cdot\text{m}^{-1}\cdot\text{K}^{-1}$  [18,19], remains well above the threshold for high-performance insulation materials, which usually have a thermal conductivity below 0.03  $\text{W}\cdot\text{m}^{-1}\cdot\text{K}^{-1}$  [20]. Consequently, while unfired earth excels at heat storage, it offers limited insulation, posing a significant scientific challenge: how to enhance its thermal performance without compromising its mechanical and environmental benefits.

One promising avenue of research involves integrating phase change materials (PCMs). These materials can absorb and release thermal energy during phase transitions from solid to liquid and vice versa, thereby increasing the thermal inertia of building envelopes and reducing indoor temperature fluctuations.

The effectiveness of a phase change material (PCM) is strongly governed by its phase transition temperature, which should match the indoor thermal comfort range to maximize latent heat storage and release. For residential buildings, the optimal PCM melting temperature is generally reported to lie between 22 and 28 °C, corresponding to typical indoor comfort conditions [21–23].

Among bio-based PCMs, coconut oil has attracted considerable attention because its melting temperature, typically ranging from 22 to 27 °C, falls within this optimal comfort range. In addition, coconut oil exhibits good thermal stability, low supercooling, and a latent heat of fusion suitable for passive thermal energy storage applications in buildings, making it a promising candidate for indoor temperature regulation [24].

However, incorporating coconut oil into construction materials requires an effective containment method to prevent leakage during phase changes. Encapsulation within polylactic acid (PLA), a biodegradable and biosourced polymer, offers a practical solution that balances durability, environmental friendliness, and mechanical stability [25,26].

In this context, the current study explores heat transfer mechanisms within unfired earth bricks containing phase change materials, with particular focus on thermal conduction and the processes of latent heat storage and release. The aim is to evaluate how thermophysical properties influence heat transfer across the brick's thickness and to assess the potential of PCMs to boost the thermal performance of unfired earth. Special attention is given to analyzing thermal phase shifts, the attenuation of temperature peaks, and the capacity for thermal energy storage. Ultimately, this research seeks to identify optimal configurations for integrating PCMs into unfired earth materials, enhancing their use in high thermal inertia building envelopes. More broadly, it contributes to the advancement of sustainable construction solutions by exploring the synergistic potential of geosourced materials and passive thermal energy storage technologies.

Haut du formulaire

## 2. Materials and Methods

The geometry studied is representative of a standard perforated fired brick measuring  $220 \times 105 \times 55$  mm, featuring 17 cylindrical cavities of 18 mm diameter distributed across three rows. This type of commercial fired brick is widely used in the construction sector, both as an interior or exterior wall cladding and as a structural element, load-bearing wall, column casing, or jamb, owing to its good mechanical properties and relatively low weight.

In the present study, brick is made of unfired earth, a natural and ecological building material whose thermal properties are particularly well-suited to the passive regulation of thermal comfort in buildings. The material selected is unfired earth, whose thermophysical properties were characterised in a previous study [17]. The cylindrical cavities are filled either with air or with a phase change material (PCM), whose integration aims to exploit the latent heat of fusion to attenuate daily thermal fluctuations within the wall. Coconut oil was selected as the PCM on account of its melting temperature ( $\approx 21$  to  $27^\circ\text{C}$ ) falling within the thermal comfort range ( $20$ – $24^\circ\text{C}$  in winter /  $23$ – $26^\circ\text{C}$  in summer [27]) and its availability as a biosourced material.

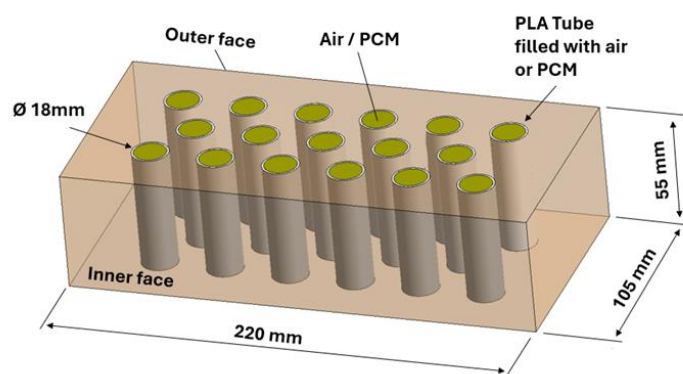


**Figure 1.** Dimensional characteristics of adobe bricks.

The main thermophysical and mechanical properties of the raw earth used to make the bricks are summarized in Table 1 [17]. The material properties are derived from analyses conducted on adobe samples collected from demolition and renovation sites of old homes and barns [17]. The raw earth under consideration has a dry density of  $1693 \text{ kg/m}^3$ . From a hygrothermal perspective, its thermal conductivity of  $0.799 \text{ W/(m}\cdot\text{K)}$  ( $\pm 0.054$ ) is relatively low. Its thermal diffusivity of  $0.479 \times 10^{-6} \text{ m}^2/\text{s}$  and its specific heat capacity of  $0.969 \text{ kJ/(kg}\cdot\text{K)}$  indicate a notable ability to store and slowly release heat, thereby promoting the thermal inertia of the wall and helping to mitigate temperature fluctuations within the building.

**Table 1.** Thermophysical properties of the raw earth [17]. The values in parentheses represent the standard deviations.

Average Physical and Thermal Properties	
$\rho_{\text{Dry}}$ ( $\text{kg/m}^3$ )	1693 (24)
Porosity	23.4 % (1.2)
Mechanical Properties	
Peak stress $f_c$ (MPa)	2.32 (0.33)
Corresponding strain $\epsilon_u$ (%)	7.10 (1.42)
Mean tangent modulus $E$ (MPa)	49.0 (4.5)
Hygrothermal Properties	
Thermal conductivity $\lambda$ ( $\text{W/mK}$ )	0.799 (0.054)
Diffusivity $a$ ( $10^{-6} \text{ m}^2/\text{s}$ )	0.479 (0.029)
Specific heat capacity $C_p$ ( $\text{kJ/(kgK)}$ )	0.969 (0.008)

### 2.1. Phase Change Material

Refined coconut oil was selected as a phase-change material (PCM) because its transition temperature ranges from 22 to 27 °C [24], making it suitable for thermal management applications in buildings. The thermophysical properties of refined coconut oil used in this study are taken from the study by Kahwaji & White [28], who performed DSC measurements and determined coconut oil's heat capacity and thermal conductivity as functions of temperature.

A density of 920 kg·m<sup>-3</sup> was adopted for coconut oil, consistent with values reported in the literature generally ranging from 920 to 925 kg·m<sup>-3</sup> depending on temperature and composition [29].

The main thermophysical characteristics of refined coconut oil are summarized in Table 2.

**Table 2.** Thermophysical properties of refined coconut oil from Kahwaji & White [28].

Melting T(°C)	Thermal Conductivity (W/mK)		Specific Heat (KJ/KgK)		Latent Heat (KJ/Kg)
	Solid Phase	Liquid Phase	Solid Phase	Liquid Phase	
24.5	0.19	0.17	1.6	2.2	105

### 2.2. PCM Encapsulation

To ensure the containment of the PCM in its liquid state and the durability of the composite, coconut oil is encapsulated in tubes printed from polylactic acid (PLA), a biodegradable, bio-based polymer [30]. The tubes, manufactured via 3D printing, have a wall thickness of 1 mm. The thermophysical properties of the PLA used in this study are (see Table 3): a density of 1250 kg·m<sup>-3</sup>, a thermal conductivity of 0.13 W·m<sup>-1</sup>·K<sup>-1</sup> close that of the coconut oil, and a specific heat capacity of 1.8 kJ·kg<sup>-1</sup>·K<sup>-1</sup> [30]. To counteract the porosity issues inherent to 3D-printed PLA, beeswax can be heated to a liquid state and brushed onto the inner walls of the tube, correcting these micro-defects to ensure a tight seal.

**Table 3.** Thermophysical properties of PLA [30].

Thermal conductivity (W/mK)	Density (kg/m <sup>3</sup> )	Specific Heat (KJ/KgK)
0.13	1250	1.8

### 2.3. Specific Experimental Protocol to Qualify the PCM Behavior

In order to characterize the thermal behavior of the PCM and to provide reference data for numerical model validation, experimental tests were conducted under controlled thermal loading. Figure 2 illustrates the equipment used. Coconut oil, previously brought to a liquid state, was introduced into a 1 mm thick PLA tube with an inner diameter of 24 mm. This tube was then inserted into the well of a ScanSense TC65M calibration furnace, which consists of a brass heating block whose inner diameter perfectly matches the outer diameter of 26mm of the tube. The applied thermal cycle consisted of imposing a temperature of 35 °C; once this target was reached, the furnace was turned off to initiate the cooling phase. The temperature evolution of the PCM was measured continuously using a K-type thermocouple positioned at mid-height of the tube, while a second thermocouple was placed at the brass/PLA interface to monitor the temperature imposed by the heating block.

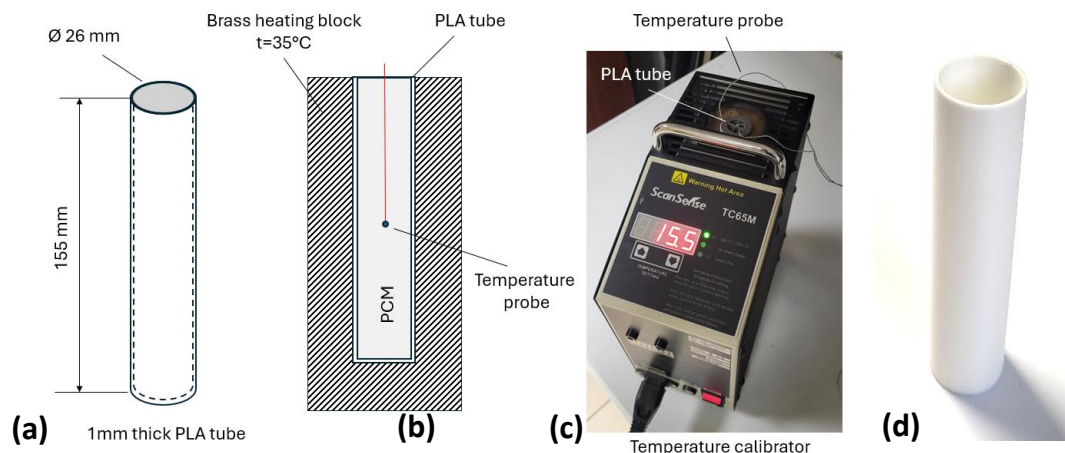


**Figure 2.** Illustration of the PLA tube filled with coconut oil (a), positioning of the thermocouple within the calibration furnace well (b), calibration furnace used for the experiment (c), and photograph of the 3D-printed PLA tube (d).

## 2.4. Numerical Methods

### 2.4.1. Problem Definition and Computational Setup

For the purposes of the numerical study, a computer-aided design (CAD) model was developed by faithfully reproducing the geometric characteristics of a commercial standard-sized perforated brick ( $220 \times 105 \times 55 \text{ mm}^3$ ) featuring 17 cylindrical cavities. The detailed dimensions, shown in Figure 1, were strictly followed to ensure a realistic representation of the coupled heat transfer phenomena between the solid raw earth matrix, the PLA containers, and the phase change material (PCM), the latter being modeled as a liquid in the simulations.

Figure 3 presents the numerical protocol implemented to evaluate thermal storage efficiency and the influence of the number of PCM rows on the thermal and energy response of the brick. The study compares a reference solid brick with four configurations incorporating an increasing number of PCM-filled rows: Case 1, containing no PCM and three air-filled rows; Case 2, containing one PCM-filled row; Case 3, containing two PCM-filled rows; and Case 4, containing three PCM-filled rows.

In order to further analyze thermal inertia and explore a solution better suited for potential industrialization, the 17 individual tubes, each with a capacity of 11mL, were subsequently replaced by a single container of equivalent volume, namely 187 mL. This container has a length of 169 mm, a width of 19 mm, and a height of 59 mm, with both lateral faces featuring a rounded edge with a radius of 0.01m. To optimize the compromise between thermal performance and mechanical integrity, this container was positioned near the exterior face subjected to the thermal loading, while maintaining sufficient distance to avoid compromising the structural strength of the brick. More specifically, it is located at one-third of the total depth of the brick, measured from the heated exterior face—a positioning chosen to maximize the early absorption of the incident heat flux while limiting mechanical stress concentrations.

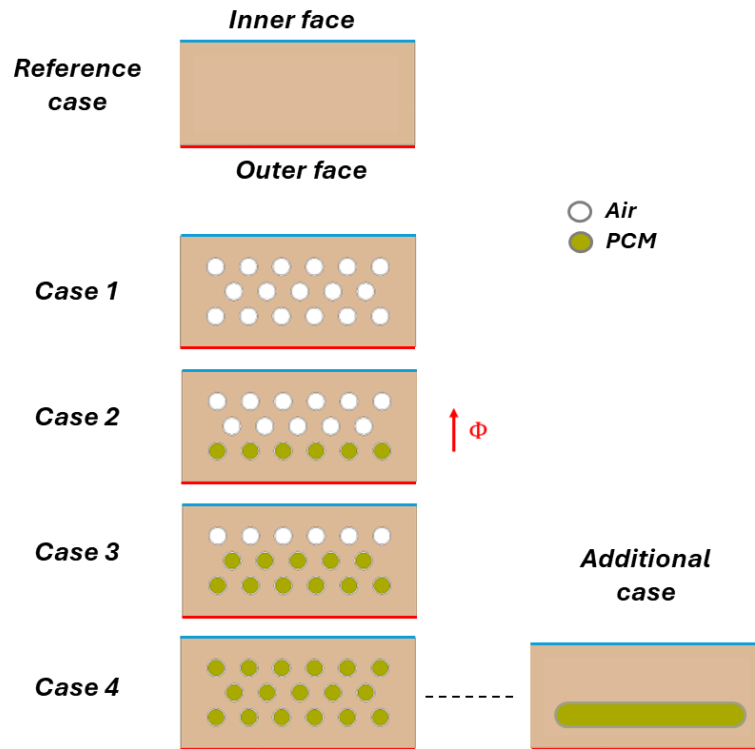


**Figure 3.** Schematic of the numerical configurations. The setup compares a reference case (full brick) to configurations incorporating 3 rows of air, followed by 1, 2, or 3 rows of Phase Change Material (PCM), with the remaining rows filled with air. For the additional case, the 17 tubes are replaced by a container with a capacity equivalent to the three rows of tubes.

#### 2.4.2. Physical Model and Governing Equations

The simulations were performed using the ANSYS Fluent® 2026R1 computational code, which is based on the finite volume method. Heat transfer is modeled in a transient regime using the general energy conservation equation. In Fluent, the temperature field is obtained from the following equation:

$$\rho c_p \frac{\partial T}{\partial t} = \nabla \cdot (k \nabla T) + S_T \quad (1)$$

where

- $\rho$  is the density of the material ( $\text{kg} \cdot \text{m}^{-3}$ ),
- $c_p$  is the specific heat capacity ( $\text{J} \cdot \text{kg}^{-1} \cdot \text{K}^{-1}$ ),
- $k$  is the thermal conductivity ( $\text{W} \cdot \text{m}^{-1} \cdot \text{K}^{-1}$ ),
- $S_T$  is a source term associated with heat release or absorption ( $\text{W} \cdot \text{m}^{-3}$ ).

For the phase change material, the Solidification/Melting enthalpy model is used. The total enthalpy  $h$  is defined by:

$$h = h_{ref} + \int_{T_{ref}}^T c_p(T') dT' + f_l L \quad (2)$$

with

- $h_{ref}$  is the enthalpy at a reference temperature  $T_{ref}$ ,
- $L$  is the latent heat of fusion ( $\text{J} \cdot \text{kg}^{-1}$ ),
- $f_l$  is the liquid fraction (ranging from 0 to 1).

The evolution of the liquid fraction is described by a linear relationship as a function of temperature:

$$f_l = \begin{cases} 0 & \text{if } T < T_S \\ \frac{T - T_S}{T_1 - T_S} & \text{if } T_S \leq T \leq T_1 \\ 1 & \text{if } T > T_1 \end{cases} \quad (3)$$

where  $T_5$  and  $T_1$  are the temperatures at the onset and completion of melting, respectively.

The energy equation then becomes:

$$\frac{\partial(\rho h)}{\partial t} = \nabla \cdot (k \nabla T) \quad (4)$$

The solution of this equation makes it possible to simultaneously track the variation in temperature and the progression of the liquid phase over time. The conduction term is treated using the local thermal conductivity of the material (brick or PCM). Interfaces between materials are handled automatically by Fluent using continuity conditions for temperature and heat flux.

To ensure an accurate representation of the thermal behavior of the materials constituting the brick, a specific database was created within the CFD code. The thermophysical properties of the raw earth and PLA, considered constant over the studied temperature range, were directly incorporated into this database using values obtained experimentally or from the literature.

In contrast, coconut oil, as a phase change material, exhibits thermophysical properties that strongly depend on temperature, particularly near its melting range. To account for this variability, user-defined functions (UDFs) were developed and implemented in the solver. These UDFs describe the temperature-dependent evolution of five key PCM properties: specific heat capacity, thermal conductivity, enthalpy, density, and dynamic viscosity. This approach enables accurate capture of the melting and solidification phenomena of coconut oil during the thermal cycle, especially the discontinuity in properties associated with the phase change.

#### 2.4.2. Computational Domain and Mesh

The computational domain was discretized using a hybrid tetrahedral–hexahedral mesh of approximately 1.2 million elements, with local refinement at the brick/PCM interfaces and exposed surfaces, as shown in Figure 4.

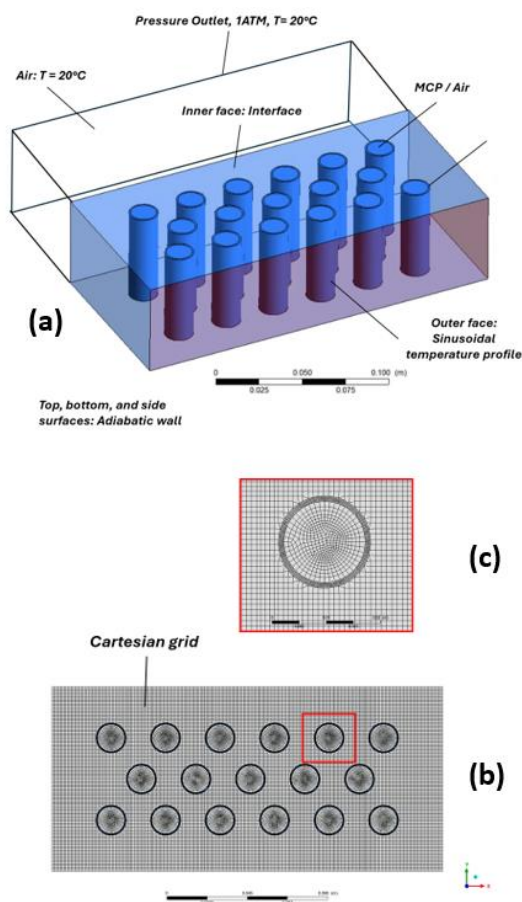


**Figure 4.** Schematic representation of the brick and thermal boundary conditions (a); mesh representation in a median xy-plane (b), and detailed view of the mesh around and inside the PLA tubes (c).

To verify the numerical accuracy of the CFD model, a mesh independence analysis was conducted using four different mesh resolutions for the configuration with three air-filled rows (Figure 5). A constant temperature of 50 °C was applied to the outer surface of the brick under steady-state conditions, and the resulting temperature on the inner surface was monitored. The sensitivity of the solution to mesh refinement was evaluated based on the average temperature of the inner face. The results show that a mesh size of 1 mm provides a satisfactory balance between accuracy and computational efficiency. Additional refinement resulted in a temperature variation of less than 0.01 °C, despite a significant increase in the number of mesh elements and computational requirements.

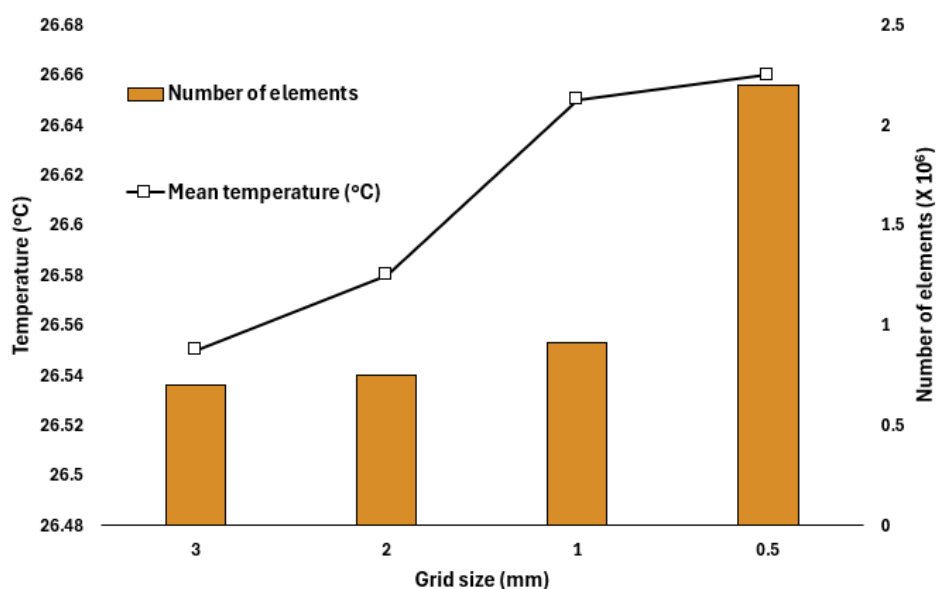


**Figure 5.** Mesh independence study for four tested grid sizes: variation in the number of elements as a function of mesh size, along with the average temperature on the inner surface of the brick. The temporal convergence of each simulation is validated once the monitored temperature stabilizes over time.

#### 2.4.3. Boundary Conditions

The temperature of the outer face of the brick (Figure 6) is imposed using a user-defined function (UDF) that reproduces the variation of the external temperature of the brick according to a diurnal cycle. It is worth noting that the maximum temperature value of 50°C is consistent with temperatures measured on building surfaces exposed to significant solar radiation during the summer period.

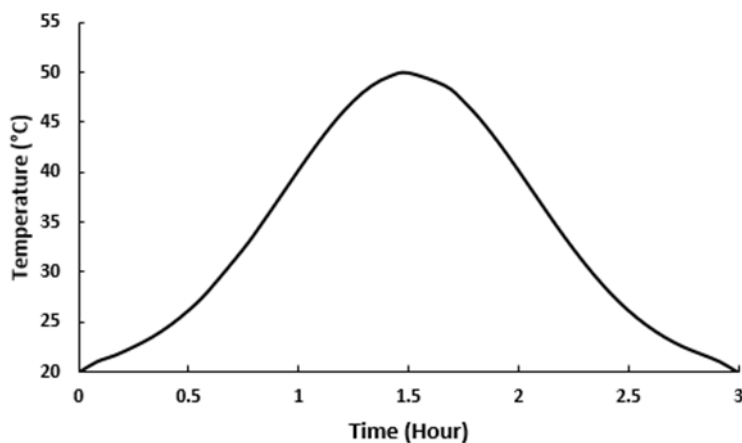


**Figure 6.** Evolution of the imposed temperature profile on the outer surface of the brick.

Table 4 summarizes the boundary conditions of the problem.

Thermal radiation between the internal cavity surfaces and the brick walls was neglected in the present numerical model. This assumption is considered acceptable because the imposed boundary conditions describe heat transfer mainly through conduction and convection mechanisms, while radiative effects remain of secondary importance under moderate temperature differences [31,32].

**Table 4.** Summary of the boundary conditions of the CFD problem.

Zone / Surface	Boundary Type	Thermal Condition	Value / Expression	Physical Remarks
Outer face (heated)	Wall	Imposed temperature	Temperature varying according to a sinusoidal law $T(t)$	Simulates the daily variation of the external temperature
Inner face (exposed to air)	Interface	Convection	—	Natural convection with ambient air ( $T = 20^{\circ}\text{C}$ )
Upper, lower, and lateral faces (left/right)	Wall	Adiabatic	$q = 0$	Laterally insulated walls
Internal interfaces (brick-PCM / brick-internal air)	Coupled	Heat flux by conduction	Continuous (Fourier's law)	Internal heat exchange solid/fluid or solid/PCM
Air zone	Pressure Outlet	—	$P = 1 \text{ atm}, T = 20^{\circ}\text{C}$	Constant pressure and temperature

#### 2.4.4. Numerical Parameters and Solutions

The simulations are carried out over a total duration of 10,800 s (3 hours), which represents a time-compressed version of the 24-hour diurnal cycle. This reduction in simulated time significantly limits the computational cost while preserving the representativeness of the physical phenomena under study, since the temperature variation imposed on the outer wall accurately reproduces the daily thermal dynamics experienced by the brick.

A time step of 5 s was selected as a satisfactory compromise between temporal resolution accuracy, fine enough to capture the dynamics of heat transfer within the brick and the cavities, and the computational cost associated with simulating the full cycle. The equations are discretized using second-order schemes, and pressure-velocity coupling is ensured by the SIMPLE algorithm.

The convergence criteria are set to  $10^{-6}$  for energy and  $10^{-4}$  for the other equations. The computations were performed on a multiprocessor workstation (Dell Precision 7920, 24 cores, 3.2 GHz, 384 GB RAM), with one full cycle requiring approximately 10 hours of computation time.

#### 2.4.5. Validation of the Numerical Model from Experimental Data

The objective of this study is to simulate heat transfer in a hollow adobe brick whose 17 cylindrical cavities are filled with either air or a phase-change material (PCM), specifically coconut oil. To validate the numerical method, we assessed the ability of the model to reproduce the behavior of a phase change material subjected to a thermal cycle. To generate the reference experimental data, a calibration furnace was used to ensure uniform heating of the walls of a PLA tube filled with coconut oil. This setup, detailed in Figure 2, made it possible to measure in real time the temperature evolution at the core of the PCM as well as the thermal kinetics imposed by the cycle.

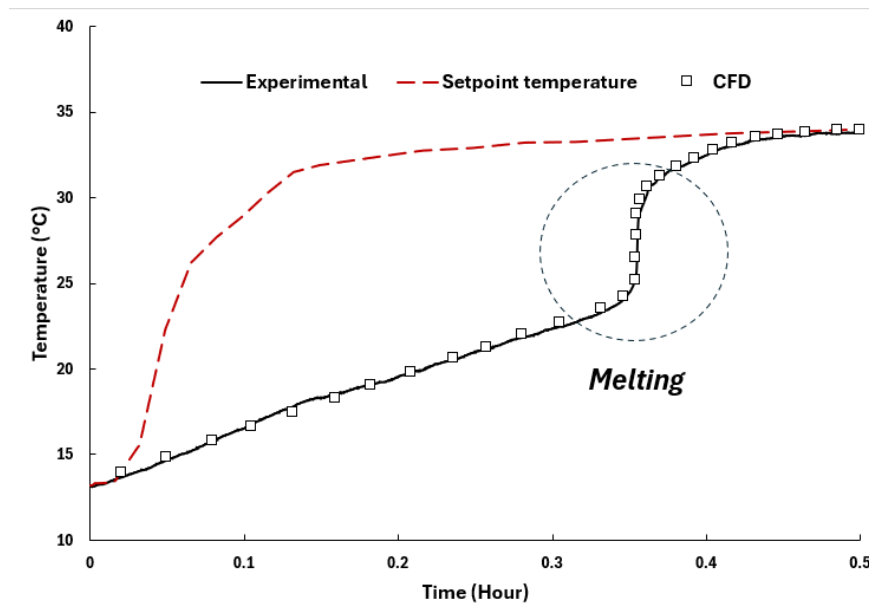


**Figure 7.** Comparison between the CFD simulation results and the experimental measurements obtained during the uniform heating of the phase change material.

Figure 7 presents a comparison between the results obtained from the numerical simulation (CFD) and the experimental measurements for this uniform heating. The red dashed curve represents the evolution of the furnace chamber temperature (setpoint temperature) during the heating process. A rapid temperature increase is observed during the first few minutes, reaching approximately 32 °C within about 10 min, followed by a slower rise toward the final setpoint of nearly 34 °C. This heating profile imposes a transient thermal excitation on the PCM sample. In contrast, the temperature of the coconut-oil-based PCM exhibits a delayed response due to its thermal inertia. During the initial heating stage, the temperature increases progressively and almost linearly from the initial temperature up to approximately 24°C, corresponding to the onset of melting. This stage reflects sensible heat storage in the solid phase. A marked change in the thermal response is then observed in the temperature range associated with phase transition. Around the melting temperature, the experimental curve exhibits a characteristic slope break followed by a sharp temperature increase, indicating the progressive solid–liquid transformation of coconut oil. This behavior results from the latent heat absorption process, during which thermal energy is primarily used for phase change rather than for increasing temperature. Once the melting process is nearly complete, the temperature rises rapidly and asymptotically approaches the furnace setpoint.

The CFD predictions reproduce this transient thermal behavior with very good accuracy over the entire heating period. In particular, the numerical results accurately capture the three main stages of the thermal response: (i) sensible heating in the solid phase, (ii) the phase transition region around 24 °C, and (iii) post-melting heating in the liquid phase. The sharp temperature rise observed experimentally during the melting interval is also well predicted, demonstrating that the model correctly reproduces the latent heat effects and the associated non-linear thermal dynamics. The slight deviations observed in the transition region may be attributed to simplifications in the numerical assumptions, such as the idealized thermophysical properties or the treatment of phase transition over a narrow melting range. Nevertheless, the overall agreement between experimental measurements and CFD results remains excellent, confirming the suitability of Fluent’s enthalpy–porosity formulation along with customized User Defined Functions (UDF) for modeling the melting behavior of coconut oil.

This validation demonstrates that the CFD model is able to reliably reproduce transient heat transfer and phase change phenomena in the PCM. It therefore provides a robust basis for subsequent numerical investigations of the thermal performance of earth-based bricks incorporating coconut-oil phase change materials.

### 3. Results and Discussion

#### 3.1. Numerical Results

##### 3.1.1. Impact of the Number of MCP Layers on Thermal Stability

Figure 8 presents the evolution of the temperature on the inner face of the brick together with the variation of the external temperature. The results clearly demonstrate the influence of the number of PCM layers on the thermal regulation performance of a wall subjected to daily temperature fluctuations.

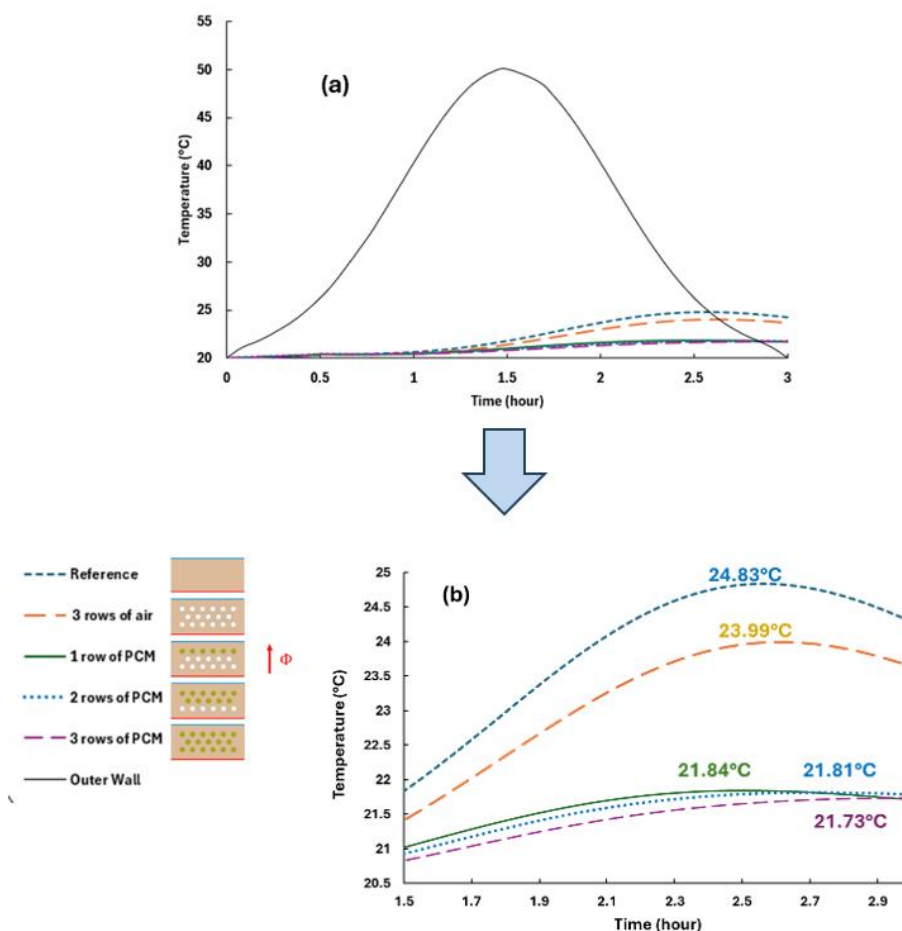


**Figure 8.** Numerical results of the brick's thermal behavior: evolution of the temperature imposed on the outer face alongside the resulting temperature on the inner face for the different configurations studied, with and without PCM (a). Detailed focus on the temperature evolution on the inner face for the configurations with PCM (b).

In the reference configuration (full brick), the inner-face temperature follows the trend of the outer face with a distinct phase shift, reaching a maximum of approximately 24.8 °C after about 2 hours 30 minutes. This behavior reflects significant heat transfer through the wall and highlights the thermal inertia limitations of the baseline raw earth brick. Compared to the full brick, the addition of three rows of air-filled cylindrical cavities induces a noticeable thermal damping effect, dropping the maximum temperature to 23.99 °C, which represents a reduction of more than 0.8 °C in peak temperature. This is primarily driven by the thermal conductivity of air ( $\sim 0.02 \text{ W}\cdot\text{m}^{-1}\cdot\text{K}^{-1}$ ), which is substantially lower than that of raw earth ( $0.799 \text{ W}\cdot\text{m}^{-1}\cdot\text{K}^{-1}$ ). The integration of a single PCM layer further reduces the thermal amplitude ( $T_{\text{max}} \approx 21.84 \text{ °C}$ ), with a slight additional improvement when

using two layers ( $T_{\max} \approx 21.81$  °C). The optimum is achieved with three layers ( $T_{\max} \approx 21.73$  °C). These results demonstrate that a higher number of PCM rows progressively enhances the latent heat storage capacity of the system.

These results are consistent with numerous studies in the literature that have demonstrated that incorporating PCMs into building walls affects thermal inertia and reduces the amplitude of indoor temperature fluctuations [33,34]. The multilayer configuration appears to be a particularly effective strategy for maximizing latent heat storage without saturation, in agreement with previous works focusing on optimizing the number of PCM layers in composite wall systems [35,36].

### 3.1.2. Spatial Distribution of Thermal Attenuation According to Layer Position

Figure 9 shows the temperature profiles plotted through the thickness of the brick along the vertical y-axis (left graph), as well as the profiles plotted along the horizontal x-axis across the three rows of cavities for the three-row PCM configuration (right graph).

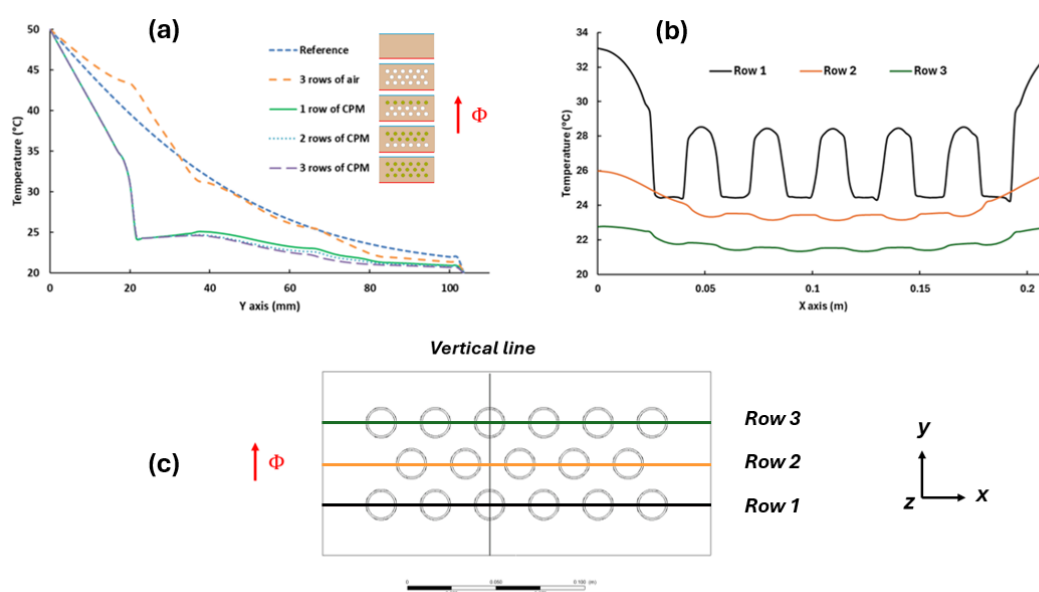


**Figure 9.** (a) Comparison of the temperature evolution plotted along a vertical axis for the different configurations studied. (b) Comparison of the temperature evolution plotted along a horizontal axis passing through each row of cavities (Row 1, Row 2, and Row 3) for the configuration with 3 PCM layers at  $t = 5400$  s (1 h 30 min), corresponding to the peak external temperature.

In the vertical profile, all configurations exhibit a monotonic decrease in temperature from the outer face (50°C) to the inner face (~20°C), with the shape and slope directly governed by the thermal conductivity of the materials involved. The full brick (reference case), composed solely of raw earth ( $\lambda = 0.799$  W/m·K), shows the most uniform gradient and the highest inner surface temperature, indicating an uninterrupted conductive heat transfer through the wall. The configuration with three rows of air cavities exhibits higher thermal resistance than the reference case, since air is a very poor conductor. This results in a steeper temperature profile within the earth regions and a more pronounced drop across the cavities.

The PCM-based configurations show a distinctive behavior: a clear temperature plateau appears around 24–25°C within the cavity zones, which is characteristic of the phase change process of coconut oil, whose melting temperature is 24.5°C. This plateau results from the absorption of latent heat by the PCM, which maintains an almost constant temperature locally until the phase transition is complete.

The slight temperature fluctuations observed in the horizontal profile (right graph) reflect the alternation of materials along the path: peaks correspond to raw earth zones ( $\lambda = 0.799$  W/m·K, conductive), while troughs correspond to PLA tubes ( $\lambda = 0.13$  W/m·K) and PCM ( $\lambda = 0.19$  W/m·K in solid state,  $0.17$  W/m·K in liquid state), both significantly less conductive.

The analysis by row reveals that Row 1, located closest to the hot outer surface, is the most actively engaged layer: its temperature fluctuates significantly around the melting temperature ( $23.8^\circ\text{C}$ ), indicating that the coconut oil is actively undergoing phase change and absorbing latent heat. In contrast, Row 2 and Row 3, further from the heat source and protected by Row 1 and the intervening earth layer, exhibit significantly lower temperatures and much smaller fluctuations. This suggests that the PCM in these deeper layers remains mostly in the solid state and is therefore much less thermally activated.

These results highlight that the effectiveness of PCM strongly depends on its position within the wall thickness and its proximity to the heat source.

### 3.2. Thermal Performance Metrics

The thermal behavior of the modified bricks was evaluated in terms of reduction in maximum inner surface temperature, temperature fluctuations, and thermal phase shift.

The damping of temperature fluctuations, commonly referred to as the decrement factor (DF), indicates the ability of the bricks to attenuate temperature variations by considering the maximum and minimum values of both the inner and outer surfaces, according to Equation (5) [37]:

$$\text{Decrement factor} = \frac{T_{i,max} - T_{i,min}}{T_{o,max} - T_{o,min}} \quad (5)$$

where  $T_{i,max}$  and  $T_{i,min}$  refer to the maximum and minimum temperatures on the inner surface of the test bricks over the entire thermal cycle. Similarly,  $T_{o,max}$  and  $T_{o,min}$  represent the maximum and minimum temperatures on the outer surface of the test bricks (in  $^\circ\text{C}$ ).

**Table 5.** Decrement factors for different configurations.

Configuration	$T_{i,max}$ ( $^\circ\text{C}$ )	$T_{i,min}$ ( $^\circ\text{C}$ )	$\Delta T_i$ ( $^\circ\text{C}$ )	Decrement factor	Amplitude reduction (%)
Full brick	24.83	20	4.83	0.247	83.9
3 air rows	23.99	20	3.99	0.204	86.7
1 PCM row	21.84	20	1.84	0.094	93.8
2 PCM rows	21.81	20	1.81	0.092	94.0
3 PCM rows	21.73	20	1.73	0.088	94.2

A decrement factor value close to zero indicates excellent thermal damping capacity, reflecting a strong attenuation of temperature fluctuations between the outer and inner surfaces of the wall. In the present case, for an extreme external temperature oscillation of  $30^\circ\text{C}$ , the results summarized in Table 5 clearly show that increasing the number of PCM layers leads to a progressive and significant reduction in the amplitude of thermal fluctuations. The decrement factor decreases from 0.247 for the reference configuration to 0.088 for the three-layer configuration. This reduction highlights the effectiveness of coconut oil in storing heat through phase change, thereby contributing to the stabilization of indoor temperature.

These results are in excellent agreement with the work of Mahdaoui et al. [38], who showed that a hollow brick impregnated with PCM enables a significant stabilization of the inner surface temperature and a substantial reduction in the decrement factor. Similarly, recent studies on earth-based walls incorporating PCMs report a significant reduction in daily thermal amplitude due to increased latent thermal inertia [39].

### 3.2.1. Time Lag

The phase shift of the peak temperature, commonly referred to the time lag, is another parameter to be evaluated, accounting for the time difference at which the peak temperature is reached on the inner and outer surfaces of the bricks [37]. Mathematically, the time lag was calculated using Equation (6), where  $\tau_{T_{i,max}}$  denotes the time at which the maximum temperature occurs on the inner surface, while  $\tau_{T_{o,max}}$  is the time at which the maximum temperature occurs on the outer surface of the bricks (in minutes).

$$\text{Time lag} = \tau_{T_{i,max}} - \tau_{T_{o,max}} \quad (6)$$

**Table 6.** Summary of Thermal Performance.

Configuration	Peak hour (h)	Time Lag (h)	Trend (h) / Ref.
<b>Full brick</b>	2 h 33 min	~1 h 03 min	
<b>3 air rows</b>	2 h 36 min	~1 h 06 min	+ 3 min
<b>1 PCM row</b>	2 h 30 min	~1 h	- 3 min
<b>2 PCM rows</b>	2 h 42 min	~1 h 12 min	+ 9 min
<b>3 PCM rows</b>	3 h	~1 h 30 min	+ 27 min

The analysis of Table 6 highlights significant differences between the studied configurations in terms of time lag. The full brick, used as a reference, shows a time lag of approximately 1 h 03 min, with a peak internal surface temperature reached at 2 h 33 min. This result serves as the comparison baseline from which the contribution of the cavities, whether filled with air or PCM, is evaluated.

The configuration with three rows of air slightly improves the time lag (+3 min compared to the reference), bringing the time lag to approximately 1 h 06 min. Although air is a poor thermal conductor, its limited phase-shifting effect is explained by the absence of latent heat energy storage: air can only delay heat transfer through conductive resistance, without any active storage mechanism.

The configurations incorporating PCM exhibit contrasting behaviors depending on the number of rows used. The configuration with a single PCM row paradoxically shows a slightly lower time lag than the reference (−3 min). The configuration with two PCM rows significantly improves time lag (+9 min), reaching a time lag of approximately 1 h 12 min, thanks to a greater amount of PCM available to absorb latent heat. However, it is the configuration with three PCM rows that proves to be the most effective, with a time lag of 1 h 30 min and a gain of +27 min compared to the reference, an improvement of nearly 43%. This result is explained by the successive activation of the three PCM-filled cavity rows, which act as active thermal barriers absorbing the latent heat of fusion of coconut oil (23.8°C) and effectively delaying the propagation of the thermal front toward the inner face.

These results confirm that increasing the volume of PCM within the brick is an effective lever for improving the thermal phase shift of the wall, with an almost proportional relationship between the number of PCM rows and the gain in time lag. This trend is consistent with the literature [34], illustrating how latent heat delays the propagation of the thermal wave.

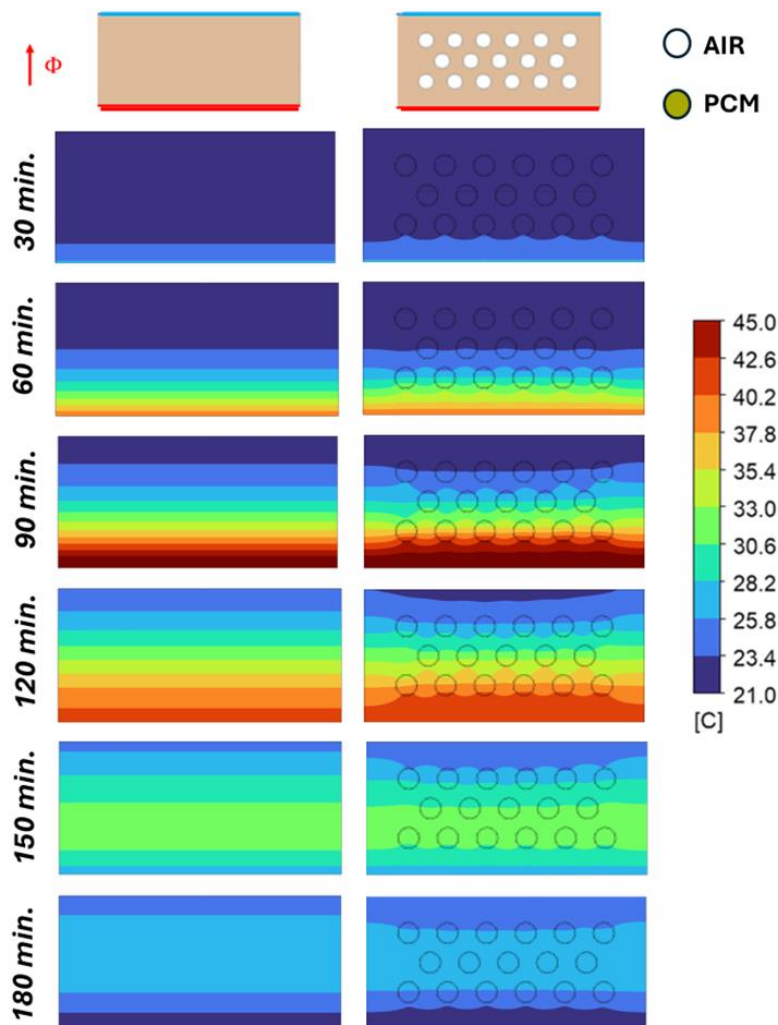


**Figure 10.** Temperature distribution in a cross-sectional plane located at mid-thickness of the brick for the full brick (reference case) and the brick with cavities filled with air. The temperature scale has been intentionally narrowed to highlight subtle temperature gradients within the brick and to better illustrate the thermal damping effect induced by the air layers.

### 3.2.2. Spatio-Temporal Analysis of the Thermal Gradient

Figure 10 and 11 highlights the spatio-temporal evolution of the temperature field across the thickness of the brick for the different configurations studied. The analysis of this thermal distribution must be interpreted in light of the thermophysical properties of the materials making up the multilayer system, namely raw earth, PLA, and the phase change material (coconut oil).

In the case of the full brick (Figure 10), the propagation of the thermal front appears relatively fast and continuous between the external and internal faces. This behavior is explained by the relatively high thermal conductivity of the brick, equal to  $0.799 \text{ W/m}\cdot\text{K}$ , associated with a thermal diffusivity of  $0.479 \times 10^{-6} \text{ m}^2/\text{s}$ . This diffusivity, which reflects the rate at which a thermal disturbance propagates through the material, promotes relatively efficient heat wave transmission across the mineral matrix. The specific heat capacity of  $0.969 \text{ kJ}/(\text{kg}\cdot\text{K})$  provides a certain sensible inertia, but this remains insufficient to significantly dampen the imposed surface thermal signal. The introduction of cavities filled with PLA and coconut oil significantly modifies the equivalent thermal resistance of the wall. PLA, used as the tube casing, has a particularly low thermal conductivity of  $0.13 \text{ W/m}\cdot\text{K}$ , nearly six times lower than that of adobe. This low conductivity acts as a first barrier to conductive heat transfer, increasing local thermal resistance and slowing the progression of the heat flux across the adobe–tube interfaces. The coconut oil used as PCM also exhibits low thermal conductivity, of  $0.19 \text{ W/m}\cdot\text{K}$  in the solid state and  $0.17 \text{ W/m}\cdot\text{K}$  in the liquid state, which is much lower

than that of the adobe matrix. From a purely conductive standpoint, this contrast in conductivity leads to a disruption of the thermal gradient at the cavity level, visible in Figure 11 as regions where the heat front noticeably slows down. However, the most decisive factor remains the thermodynamic behavior of the PCM. Refined coconut oil has a latent heat of fusion of 105 kJ/kg, associated with a melting temperature of 24.5 °C. When the local temperature is close the melting temperature, a significant portion of the incoming energy is absorbed as latent heat without a substantial increase in temperature. This phenomenon explains the quasi-isothermal zones observed in configurations incorporating one, two, or three PCM rows.

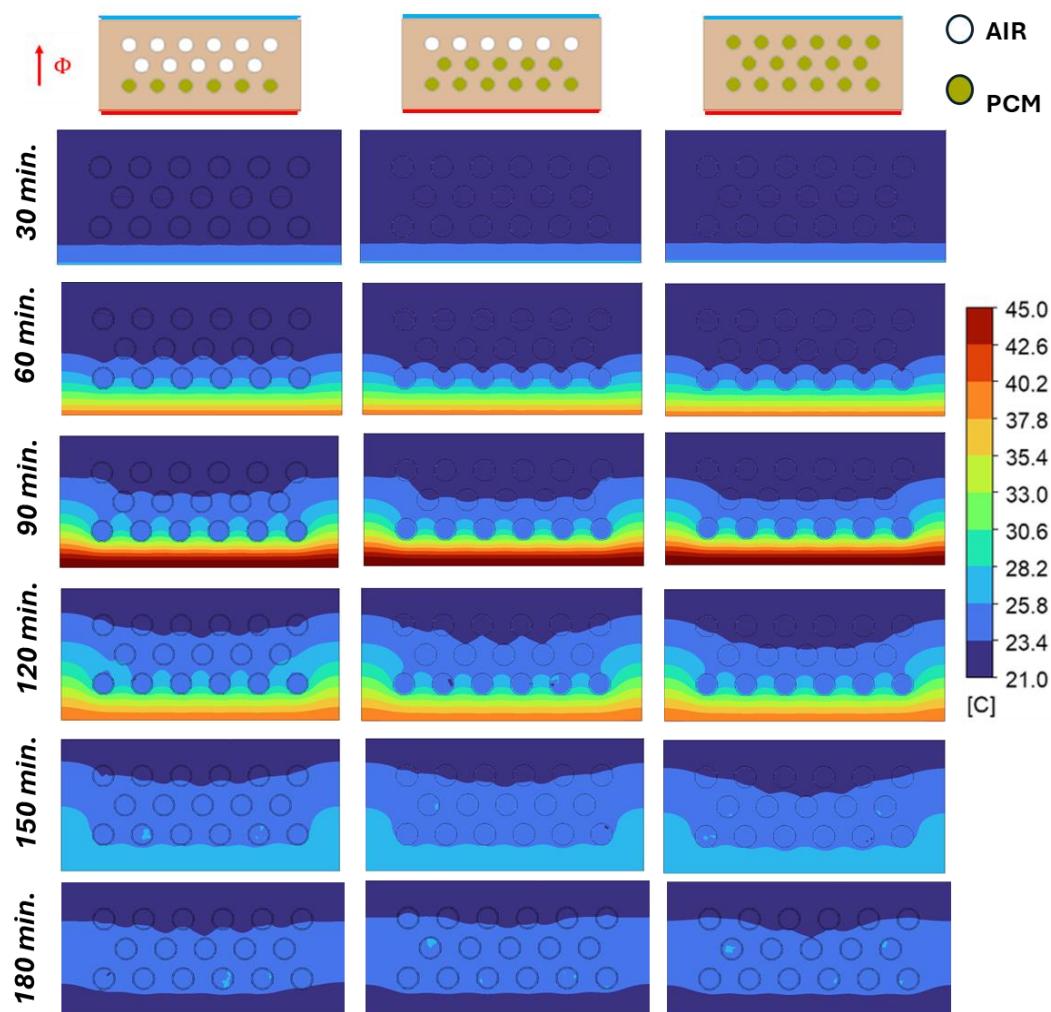


**Figure 11.** Temperature distribution in a cross-sectional plane located at mid-thickness of the brick for different configurations with PCM: one row filled with PCM, and two and three rows filled with PCM. The temperature scale has been intentionally narrowed to highlight subtle temperature gradients within the brick and to better illustrate the thermal damping effect induced by the PCM layers.

From a physical standpoint, the system behaves as a combination of thermal resistances coupled with latent energy storage capacities. This improvement results directly from the slowed propagation of the thermal front in a system of successive thermal resistances. According to Harb et al. [40], the equivalent thermal resistance can be expressed using equations (6) and (7):

$$R_{eq} = \frac{1}{U} = R_{S,i} + R_{S,e} \quad (6)$$

$$U = \frac{\Phi T}{ST(T_i - T_e)} \quad (7)$$

where  $U$  is the thermal transmittance ( $W/m^2.K$ ),  $R_{s,i}$  and  $R_{s,e}$  are respectively the inner and external surface thermal resistance due to convection ( $m^2.K/W$ );  $\Phi T$  is the total unidirectional heat flux ( $W$ ) crossing the total surface  $ST$  ( $m^2$ ),  $T_i$  and  $T_e$  are respectively the internal and external temperature ( $K$ ).

Each PCM layer acts as an active thermal barrier: heat must not only pass through low-conductivity layers but also supply the energy required for the phase transition. Increasing the number of PCM rows therefore leads to a progressive rise in this equivalent thermal resistance, while simultaneously increasing the system's energy storage capacity.

This trend is fully consistent with the literature on hollow bricks incorporating PCMs, where thermal phase shift increases with PCM mass and with the distance between the PCM and the inner face [41,42]. Recent studies have even reported time lags of several hours when PCM volume and its positioning within the wall structure are optimized [43].

In the three-row PCM configuration, the thermal front is strongly delayed in the outer half of the brick. Each row acts as an active thermal barrier, combining low conductivity and latent storage. The heat flux must successively cross the adobe-PLA-PCM interfaces, then provide the energy required for PCM melting before progressing to the next row. This multilayer architecture produces a spatio-temporal spreading of the heat front, visible in Figure 11 through a slower displacement of isotherms toward the internal face. The internal temperature thus remains much more stable, which explains the excellent performance observed in terms of decrement factor and time lag. This behavior closely resembles the temperature distributions reported in numerical studies of hollow bricks incorporating PCM in hot climates [38].

Figure 10 and 11 shows that thermal performance does not result solely from the low conductivity of the incorporated materials, but from the synergy between conductive resistance, sensible inertia of adobe, and latent storage of coconut oil. This complementarity provides the system with a thermal inertia significantly higher than that of a conventional brick. The observed performance is fully consistent with recent literature on latent heat storage building materials, while also highlighting the specific advantage of bio-based adobe as a matrix with high sensible thermal inertia [44,45].

### 3.3. Additional Case: Geometric Simplification

In light of the results obtained for the configurations with 1, 2, and 3 PCM rows, the three-row configuration appears to provide the best thermal performance among the initially studied geometries. However, the differences observed between these three configurations remain relatively small, raising the question of geometric optimization aimed at simplifying the manufacturing process.

In this context, an additional case was investigated by replacing the 17 cylindrical PLA tubes with a single container of equivalent volume. This approach aims to assess the possibility of maintaining, or even improving, thermal performance while reducing the manufacturing complexity of the bricks, with a view toward potential industrialization.

**Table 7.** Comparison of thermal performance and decrement factors between the additional case, the Full brick, and the brick with three PCM rows.

Configuration	$T_{i,max}$ ( $^{\circ}C$ )	Decrement Factor	Time Lag (h)
Full Brick	24.83	0.247	~1 h 03 min
3 rows PCM	21.73	0.088	~1 h 30 min
Equivalent container	20.87	0.044	>1 h 30 min

The results obtained and summarized in Table 7 show that this geometric simplification leads to a significant improvement in thermal performance. Indeed, the maximum temperature measured on the inner surface decreases from  $21.73^{\circ}C$  to  $20.87^{\circ}C$ , while the decrement factor drops from 0.088 to 0.044, representing an additional 50% reduction compared to the configuration with three PCM rows.

Moreover, the time lag exceeds 1 h 30 min. The analysis of the total enthalpy maps presented in Figure 12 highlights distinct thermal behavior across the three studied configurations. Total enthalpy corresponds to the sum of the sensible and latent energy of the material. It enables the modeling of heat transfer and phase change phenomena while characterizing the material's ability to absorb or release heat during a process. For the Full brick, the thermal front progresses homogeneously and continuously from the exposed face toward the inner face, with well-defined horizontal stratification bands appearing as early as 90 minutes, reflecting purely conductive diffusion without any latent storage effect. For the configuration with three rows of circular cavities (3 Rows of PCM), the maps reveal heat absorption concentrated around each capsule, with a progressive activation of the cavities from the most exposed row toward the inner rows. At 90 and 150 minutes, the cavities closest to the hot face reach high enthalpy levels (red-orange zones), while the more distant cavities remain partially underutilized, confirming a spatial heterogeneity in latent heat absorption inherent to multi-cavity geometries.

The equivalent container configuration, on the other hand, exhibits a markedly different behavior. As early as 30 minutes, the equivalent container concentrates a high-enthalpy zone within a continuous PCM volume, indicating rapid and spatially uniform absorption of latent heat. At 90 and 150 minutes, the container acts as a nearly continuous thermo-capacitive barrier across the brick thickness: the thermal front is significantly slowed at this level, resulting in a more pronounced enthalpy gradient between the exposed and inner faces, as well as a greater delay in heat transmission toward the indoor space. This behavior is consistent with recent studies showing that continuous macro-encapsulation systems enhance latent heat storage effects and improve indoor temperature stabilization in building envelopes [46], and aligns with literature emphasizing the importance of continuity in latent storage zones for improving the thermal performance of integrated bricks [34].

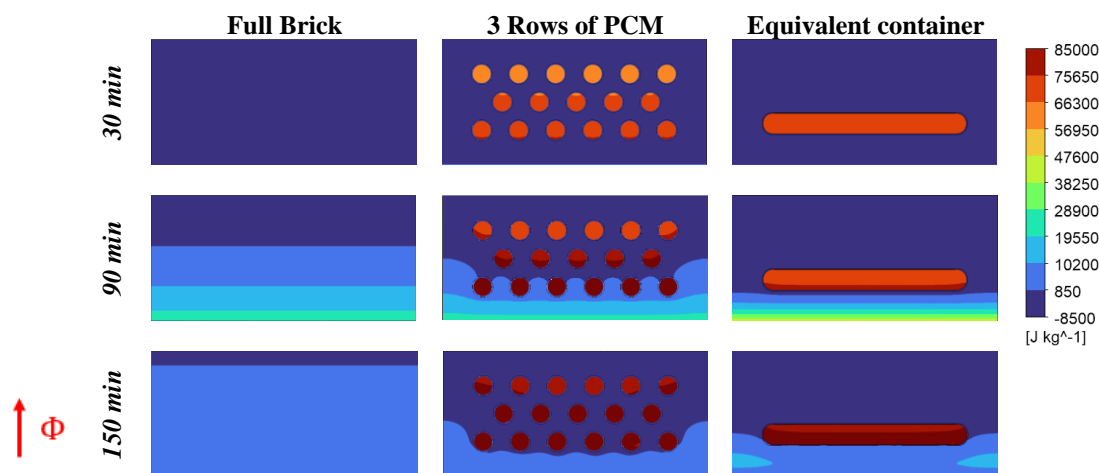


**Figure 12.** Comparison of total enthalpy distribution at three characteristic times (30, 90, and 150 min) for the reference full brick, the three-row PCM configuration, and the equivalent single-container design. The heated face is located at the bottom of each subfigure, so that the thermal front propagates from bottom to top across all configurations.

Beyond thermal performance, this solution presents significant advantages from both technological and economic perspectives. Replacing the 17 individual tubes with a single container considerably reduces the number of manufacturing and assembly operations, particularly in the 3D printing of PLA, while also decreasing the number of interfaces between the adobe, the polymer, and the PCM. This simplification is likely to limit interfacial defects, improve component reproducibility, and reduce production costs at an industrial scale. These considerations are consistent with recommendations in the literature, which identify simplified macro-encapsulation as a particularly promising pathway for the large-scale deployment of PCM in construction materials [46].

### 3.4. Limitations

First, the use of PLA as the encapsulation material raises durability concerns. Although this bio-based polymer is easy to process and suitable for 3D printing, its long-term behavior under repeated heating and cooling cycles remains uncertain. Thermal fatigue, mechanical degradation, and cracking may occur, especially under significant temperature gradients. In addition, the intrinsic porosity associated with the 3D printing process may promote moisture transfer or sealing defects, potentially affecting thermal performance and long-term system stability.

Second, the use of coconut oil as a phase change material presents limitations in terms of sustainability and regional relevance. While its thermophysical properties are favorable, it is not locally produced in Europe, leading to additional carbon emissions related to transportation and reliance on external supply chains. Furthermore, its long-term thermal stability under repeated melting/solidification cycles, as well as potential degradation mechanisms (such as oxidation or phase separation), require further investigation.

Moreover, introducing a larger cavity within the brick may induce non-negligible mechanical constraints. Such a geometry can affect compressive strength, creep resistance, and overall durability under cyclic thermo-mechanical loading. It may also generate stress concentrations around the cavity, increasing the risk of cracking in the adobe matrix.

Finally, practical and industrial considerations must be addressed, including compatibility with existing construction techniques, variability in raw earth properties, and the reproducibility of performance at a larger scale.

Therefore, despite the promising thermal results, further investigations, particularly focusing on durability, mechanical behavior, and life cycle assessment, are necessary to validate the relevance of this solution for real-world building applications.

## 4. Conclusions

This study highlights the significant potential of integrating phase change materials (PCMs) into adobe bricks to sustainably improve their thermo-energetic performance. Although adobe naturally exhibits interesting sensible thermal inertia due to its specific heat capacity and porous structure, its relatively high thermal conductivity limits its effectiveness when used alone as an envelope material. The incorporation of PCMs therefore appears to be a particularly relevant strategy to enhance thermal damping capacity and improve passive comfort in buildings.

The numerical results clearly show that increasing the number of PCM rows progressively improves the thermal response of the wall. The configuration with three PCM rows proved to be the most effective among the initially studied geometries, with a marked reduction in the maximum internal surface temperature, a decrement factor reduced to 0.088, and a time lag extended to 1 h 30 min, reflecting a substantial improvement in the system's effective thermal inertia. The spatio-temporal analysis of thermal fields and enthalpy maps made it possible to identify the physical mechanisms underlying these performances. The observed improvement results from the synergy between the sensible inertia of the adobe matrix, the low thermal conductivity of the PLA envelopes, and the latent heat storage of coconut oil during phase transition. This combination significantly slows down the propagation of the thermal front and contributes to stabilizing the internal surface temperature.

The additional case of geometric simplification, based on replacing the 17 tubes with a single container of equivalent volume, represents one of the most promising outcomes of this study. This configuration not only achieves the best thermal performance, with a decrement factor of 0.044, but also opens up concrete prospects for technological transfer and industrialization, thanks to a notable reduction in manufacturing complexity, number of interfaces, and potential production costs.

These results confirm the relevance of approaches combining bio-based materials and latent heat energy storage for the development of high-performance passive building solutions. However, further work is needed on mechanical characterization, durability under thermo-mechanical cycling,

and full-scale experimental validation in order to consolidate the viability of these bricks for real-world construction applications.

**Author Contributions:** Conceptualization, F.B. and M.L.; methodology, F.B.; software, F.B.; validation, M.L., and G.P.; formal analysis, G.P.; investigation, F.B.; writing—original draft preparation, F.B.; writing—review and editing, G.P.; visualization, M.L. All authors have read and agreed to the published version of the manuscript.

**Funding:** This research received no external funding.

**Data Availability Statement:** The raw data supporting the conclusions of this article will be made available by the authors on request.

**Conflicts of Interest:** The authors declare no conflicts of interest.

## References

1. Minke, G. *Building with Earth: Design and Technology of a Sustainable Architecture*; Birkhäuser: Basel, 2006.
2. Houben, H.; Guillaud, H. *Earth Construction: A Comprehensive Guide*; Intermediate Technology Publications: London, 1994.
3. UNESCO / CRAterre *Earth Construction: A World Heritage*; CRAterre-EAG: Grenoble, 1985.
4. Ben-Alon, L.; Loftness, V.; Harries, K.A.; DiPietro, G.; Hameen, E.C. *Cradle to site Life Cycle Assessment (LCA) of natural vs conventional building materials: A case study on cob earthen material*. *Building and Environment* **2019**, *160*, 106150. <https://doi.org/10.1016/j.buildenv.2019.05.028>[Get rights and content](#)
5. Hamard, E.; Cazacliu, B.; Razakamanantsoa, A.; Morel, J.-C. *Cob, a Vernacular Earth Construction Process in the Context of Modern Sustainable Building*. *Building and Environment* **2016**, *106*, 103–119. <https://doi.org/10.1016/j.buildenv.2016.06.009>
6. Gallipoli, D.; Bruno, A.W.; Perlot, C.; Mendes, J. *A Geotechnical Perspective of Raw Earth Building*. *Acta Geotechnica* **2017**, *12*, 463–478. <https://doi.org/10.1007/s11440-016-0521-1>
7. Walker, P.; Keable, R.; Martin, J.; Maniatidis, V. *Rammed Earth: Design and Construction Guidelines*; BRE Press, 2005.
8. Illampas, R.; Ioannou, I.; Charmpis, D.C. *Experimental assessment of adobe masonry assemblages under monotonic and loading–unloading compression*. *Materials and Structures* **2017**, *50*, 79. <https://doi.org/10.1617/s11527-016-0952-z>
9. Pacheco-Torgal, F.; Jalali, S. *Earth Construction: Lessons from the Past for Future Eco-Efficient Construction*. *Construction and Building Materials* **2012**, *29*, 512–519. <https://doi.org/10.1016/j.conbuildmat.2011.10.054>
10. Laborel-Préneron, A.; Aubert, J.-E.; Magniont, C.; Tribout, C.; Bertron, A. *Plant Aggregates and Fibers in Earth Construction Materials: A Review*. *Construction and Building Materials* **2016**, *111*, 719–734. <https://doi.org/10.1016/j.conbuildmat.2016.02.119>
11. Illampas, R.; Ioannou, I.; Charmpis, D.C. *Adobe Bricks under Compression: Experimental Investigation and derivation of stress–strain equation*. *Construction and Building Materials* **2014**, *53*, 83–90. <https://doi.org/10.1016/j.conbuildmat.2013.11.103>
12. Quagliarini, E.; Lenci, S. *The Influence of Natural Stabilizers and Natural Fibres on the Mechanical Properties of Ancient Roman Adobe Bricks*. *Journal of Cultural Heritage* **2010**, *11*, 309–314. [10.1016/j.culher.2009.11.012](https://doi.org/10.1016/j.culher.2009.11.012)
13. Piattoni, Q.; Quagliarini, E.; Lenci, S. *Experimental analysis and modelling of the mechanical behaviour of earthen bricks*. *Construction and Building Materials* **2011**, *25*, 2067–2075. <https://doi.org/10.1016/j.conbuildmat.2010.11.039>
14. Vega, P.; Juan, A.; Guerra, I.; Morán, J.M.; Aguado, P.J. *Mechanical Characterization of Traditional Adobes from the North of Spain*. *Construction and Building Materials* **2011**, *25*, 3020–3023. <https://doi.org/10.1016/j.conbuildmat.2011.02.003>
15. Silveira, D.; Varum, H.; Costa, A.; Martins, T.; Pereira, H.; Almeida, J. *Mechanical Properties of Adobe Bricks in Ancient Constructions*. *Construction and Building Materials* **2012**, *28*, 36–44. <https://doi.org/10.1016/j.conbuildmat.2011.08.046>

16. Polidori, G.; Aras-Gaudry, A.; Beaumont, F.; Bogard, F.; Murer, S.; Lachi, M.; Maalouf, C.; Moussa, T.; Bliard, C.; Fronteau, G.; et al. *Adobe Bricks of the Champagne Region (France): Characterization of a Chalky Raw Earth Construction Material*. *Materials* **2024**, *17*, 2307, doi:10.3390/ma17102307.
17. Polidori, G.; Aras-Gaudry, A.; Rousse, C.; Beaumont, F.; Bogard, F.; Murer, S.; Moussa, T.; Bliard, C.; Fronteau, G.; Hamard, E. *Analysis of adobes from vernacular raw earth buildings in the Champagne region (France)*. *Construction and Building Materials* **2025**, *470*, 140582, doi:10.1016/j.conbuildmat.2025.140582.
18. Rempel, A.R.; Rempel, A.W. *Rocks, Clays, Water, and Salts: Highly Durable, Infinitely Rechargeable, Eminently Controllable Thermal Batteries for Buildings*. *Geosciences* **2013**, *3*, 63–101. <https://doi.org/10.3390/geosciences3010063>
19. Mora-Ruiz, V.; Soto-Paz, J.; Attia, S.; Mejía-Parada, C. *Sustainable Earthen Construction: A Meta-Analytical Review of Environmental, Mechanical, and Thermal Performance*. *Buildings* **2025**, *15*, 918, doi:10.3390/buildings15060918.
20. ISO 10456:2007 Available online: <https://www.iso.org/fr/standard/40966.html> (accessed on 26 May 2026).
21. Zalba, B.; Marín, J.M.; Cabeza, L.F.; Mehling, H. *Review on Thermal Energy Storage with Phase Change Materials, heat transfer analysis and applications*. *Applied Thermal Engineering* **2003**, *23*, 251–283, doi:10.1016/S1359-4311(02)00192-8.
22. Sharma, A.; Tyagi, V.V.; Chen, C.R.; Buddhi, D. *Review on Thermal Energy Storage with Phase Change Materials and Applications*. *Renewable and Sustainable Energy Reviews* **2009**, *13*, 318–345. <https://doi.org/10.1016/j.rser.2007.10.005>
23. Akeiber, H.; et al. *A review on phase change material (PCM) for sustainable passive cooling in building envelopes*. *Renewable and Sustainable Energy Reviews* **2016**, *60*, 1470–1497. <https://doi.org/10.1016/j.rser.2016.03.036>
24. Saleel, C.A. *A review on the use of coconut oil as an organic phase change material with its melting process, heat transfer, and energy storage characteristics*. *Journal of Thermal Analysis and Calorimetry* **2022**, *147*, 3751–3771, doi:10.1007/s10973-021-10839-7.
25. Jamshidian, M.; et al. *Poly-Lactic Acid: Production, Applications, Nanocomposites, and Release Studies*. *Comprehensive Reviews in Food Science and Food Safety* **2010**, *9*, 552–571. <https://doi.org/10.1111/j.1541-4337.2010.00126.x>
26. Farah, S.; Anderson, D.G.; Langer, R. *Physical and Mechanical Properties of PLA and their functions in widespread applications — A comprehensive review*. *Advanced Drug Delivery Reviews* **2016**, *107*, 367–392. <https://doi.org/10.1016/j.addr.2016.06.012>
27. ISO 7730:2025 Available online: <https://www.iso.org/standard/85803.html> (accessed on 19 May 2026).
28. Kahwaji, S.; White, M.A. *Edible Oils as Practical Phase Change Materials for Thermal Energy Storage*. *Applied Sciences* **2019**, *9*, 1627, doi:10.3390/app9081627.
29. Al-Jethelah, M.; Al-Sammarraie, A.; Tasnim, S.; Mahmud, S.; Dutta, A. *Effect of Convection Heat Transfer on Thermal Energy Storage Unit*. *Open Physics* **2018**, *16*, 861–867, doi:10.1515/phys-2018-0108.
30. Barkhad, M.S.; Abu-Jdayil, B.; Mourad, A.H.I.; Iqbal, M.Z. *Thermal Insulation and Mechanical Properties of Polylactic Acid (PLA) at Different Processing Conditions*. *Polymers* **2020**, *12*, 2091, doi:10.3390/polym12092091.
31. Lorente, S.; Petit, M.; Javelas, R. *Simplified Analytical Model for Thermal Transfer in Vertical Hollow Brick*. *Energy and Buildings* **1996**, *24*, 95–103, doi:10.1016/0378-7788(95)00965-5.
32. Incropera, F.P., DeWitt, D.P., Bergman, T.L., Lavine, A.S., *Principles of Heat and Mass Transfer*; Eds.; 7. ed., international student version.; Wiley: Hoboken, NJ, 2013; ISBN 978-0-470-50197-9.
33. Sawadogo, M.; Duquesne, M.; Belarbi, R.; Hamami, A.E.A.; Godin, A. *Review on the Integration of Phase Change Materials in Building Envelopes for Passive Latent Heat Storage*. *Applied Sciences* **2021**, *11*, 9305, doi:10.3390/app11199305.
34. Gao, Y.; Gao, W.; Meng, X.; Long, E. *Influence of the PCM Layer Location on the Multilayer Wall Thermal Performance*. *Open Journal of Energy Efficiency* **2017**, *6*, 1–13, doi:10.4236/ojee.2017.61001.
35. Terhan, M.; Ilgar, G. *Investigation of Used PCM-Integrated into Building Exterior Walls for Energy Savings and Optimization of PCM Melting Temperatures*. *Construction and Building Materials* **2023**, *369*, 130601, doi:10.1016/j.conbuildmat.2023.130601.

36. Geng, X.; Wang, J.; Gao, Y.; Meng, X. Location Combination Optimization of Thermal Insulation Material and Phase-Change Material in Multi-Layer Walls under Air-Conditioning Continuous and Intermittent Operation. *Journal of Energy Storage* **2021**, *44*, 103449, doi:10.1016/j.est.2021.103449.
37. Toure, P.M.; Dieye, Y.; Gueye, P.M.; Sambou, V.; Bodian, S.; Tiguampo, S. *Experimental Determination of Time Lag and Decrement Factor*. *Case Studies in Construction Materials* **2019**, *11*, e00298, doi:10.1016/j.cscm.2019.e00298.
38. Mahdaoui, M.; Hamdaoui, S.; Ait Msaad, A.; Kousksou, T.; El Rhafiki, T.; Jamil, A.; Ahachad, M. *Building Bricks with Phase Change Material (PCM): Thermal Performances*. *Construction and Building Materials* **2021**, *269*, 121315, doi:10.1016/j.conbuildmat.2020.121315.
39. Jia, C.; Geng, X.; Liu, F.; Gao, Y. Thermal Behavior Improvement of Hollow Sintered Bricks Integrated with Both Thermal Insulation Material (TIM) and Phase-Change Material (PCM). *Case Studies in Thermal Engineering* **2021**, *25*, 100938, doi:10.1016/j.csite.2021.100938.
40. Harb, E.; Maalouf, C.; Bliard, C.; Tenpierik, M.; Lachi, M.; Bogard, F.; Polidori, G. *Thermal Performance of Starch/Beet-Pulp Composite Bricks for Building Insulation at a Wall Scale*. *Case Studies in Construction Materials* **2023**, *18*, e01851, doi:10.1016/j.cscm.2023.e01851.
41. Dellagi, A.; Ayed, R.; Bouadila, S.; Guizani, A. *Computational and Experimental Analysis of PCM-Infused Brick for Sustainable Heat Regulation*. *Journal of Building Physics* **2024**, *48*, 222–243, doi:10.1177/17442591241255966.
42. Kishore, R.; Bianchi, M.; Booten, C.; Vidal, J.; Jackson, R. *Parametric and Sensitivity Analysis of a PCM-Integrated Wall for Optimal Thermal Load Modulation in Lightweight Buildings*. *Applied Thermal Engineering* **2021**, *187*, 116568, doi: 10.1016/j.applthermaleng.2021.116568.
43. Ye, Q.; Ba, L.; Nguyen, G.T.M.; Absi, R.; Ledésert, B.A.; Dosseh, G.; Hebert, R.L. Experimental and Numerical Simulation Study on the Thermal Performance of Building Envelope Structures Incorporating the Solid-Solid Phase Change Material. *Energy and Buildings* **2025**, *348*, 116476, <https://doi.org/10.1016/j.enbuild.2025.116476>.
44. Lachheb, M.; Youssef, N.; Younsi, Z. A Comprehensive Review of the Improvement of the Thermal and Mechanical Properties of Unfired Clay Bricks by Incorporating Waste Materials. *Buildings* **2023**, *13*, 2314. <https://doi.org/10.3390/buildings13092314>.
45. Osibodu, S.J.; Adeyinka, A.M.; Mbelu, O.V. *PCM Integration in Concrete for Thermal Storage*. *Sustainable Energy Research* **2024**, *11*, 45, doi:10.1186/s40807-024-00138-8.
46. Liu, Z.; Yu, Z.; Yang, T.; Qin, D.; Li, S.; Zhang, G.; Haghghat, F.; Mastani Joybari, M. *A Review on Macro-Encapsulated Phase Change Material for Building Envelope Applications*. *Building and Environment* **2018**, *144*, doi:10.1016/j.buildenv.2018.08.030.

**Disclaimer/Publisher's Note:** The statements, opinions and data contained in all publications are solely those of the individual author(s) and contributor(s) and not of MDPI and/or the editor(s). MDPI and/or the editor(s) disclaim responsibility for any injury to people or property resulting from any ideas, methods, instructions or products referred to in the content.